ac-conductivity measurements on $La_2NiO_{4+\delta}$

H. Jhans, D. Kim,* R. J. Rasmussen,† and J. M. Honig
Department of Chemistry, Purdue University, West Lafayette, Indiana 47907
(Received 21 July 1995; revised manuscript received 28 March 1996)

We have carried out ac-conductivity $\sigma(\omega)$ measurements on $La_2NiO_{4+\delta}$, $0<\delta\leqslant 0.08$, in the frequency (ω) and temperature ranges 5 Hz–13 MHz and 75–300 K. The ac conductivity follows a set of basic characteristics: (i) $\sigma(\omega)$ obeys the ω^s power law ($s\sim 0.38-0.85$). (ii) At higher frequencies, $\sigma(\omega)$ saturates. To our knowledge, saturation of $\sigma(\omega)$ with ω in the radio frequency range has not been previously reported for an electronic system. (iii) $\sigma(\omega)$ is weakly temperature dependent in the dispersive region. (iv) Below the saturation region, for a fixed δ, the reduced conductivity $\sigma(\omega)/\sigma(0)$, at various values of T can be scaled to a generalized reduced frequency $\omega_n=\omega/\sigma(0)T^n$. For $\delta=0.01-0.08$, n is $=-\frac{1}{3}$ or $-\frac{1}{4}$. (v) Furthermore, at a fixed T, the reduced conductivities for various δ lie on a universal curve; n in this case varies from $-\frac{1}{4}$ to $-\frac{1}{2}$. (vi) Good agreement of data with the Summerfield extended pair approximation theory, $\sigma(\omega)/\sigma(0)=1+(A\omega\alpha e^2/\sigma(0)k_BT^n)^b$, is found; $b\sim 0.64-1$. (vii) Our data analysis reveals two loss peaks; the first is located near the critical frequency ω_c below which the imaginary part of conductivity $\sigma_2(\omega)$ is proportional to ω. (viii) The relation $\sigma(0)\propto\omega_c$ is obeyed, with $\omega_c\propto\exp[-(T_2/T)^{1/3}]$. The second loss peak lies near the onset of saturation. These characteristic signatures in the ac conductivity point to a transport mechanism involving localized states near the Fermi level. [S0163-1829(96)04540-7]

I. INTRODUCTION

We report here on ac-conductivity properties of $La_2NiO_{4+\delta}$, which, to the best of our knowledge, have not been published so far. Considerable interest attaches to this system because of its close relationship to La_2CuO_4, which belongs to the class of quasi-two-dimensional K_2NiF_4 structures. For doped and reduced La_2CuO_4 (Refs. 1–3) and Sr-doped La_2NiO_4,[4] the dc conductivity $\sigma(0)$ varies with T as T^m, where m lies in the range between $-\frac{1}{3}$ and $-\frac{1}{4}$. In later work, $La_2CuO_{4+\delta}$, $0.001\leqslant\delta\leqslant 0.01$, was reported to exhibit two-dimensional (2D) weak Anderson localization.[5] For La_2NiO_4, the 2D character was established through dc measurements on single crystals, which indicate that the conductivity of the nickelates in the NiO_2 basal plane exceeds that along the orthogonal c direction by nearly two orders of magnitude.[6] Various band-structure schemes have been advanced to rationalize the observed transport data.[7] However, it is not clear whether the charge carriers are itinerant large polarons or localized small polarons, i.e., whether the observed activation energy is due to the thermal promotion of carriers across an energy gap and/or to an activated mobility. Recent resistivity measurements[8] conducted on as-grown $La_2NiO_{4+\delta}$ ($\delta\approx 0.05$) crystals in the NiO_2 basal plane by the *potentiostatic* four-probe resistivity technique reveal that $m=-\frac{1}{3}$ over the 300–77-K range. Furthermore, ac conductivity in the basal plane exhibits dispersion in the 5-Hz–10-MHz frequency range, whereas along the c direction it is dispersionless.[8] These experiments[8] also confirm the 2D character of La_2NiO_4, and suggest that transport involves localized states. As oxygen stoichiometry affects all physical properties, we have carried out systematic investigation of the ac-conductivity characteristics of La_2NiO_4 as a function of stoichiometry.

The ac-conductivity data, in general, display a set distinct, basic characteristics, gathered from the wealth of experimental and theoretical investigations, that a large number of investigators have contributed to this field. The first theoretical investigation of Mott and Austin[9] (1969) had a number of shortcomings, which have since been addressed in several theoretical treatments on hopping transport,[10–12] using a variety of approaches, such as the effective-medium approximation,[12] effective pair approximation[13] (EPA) (Butcher and Summerfield), continuous time random-walk formalism[14] (Dyre), and percolation theory[15] (Hunt). We emphasize that these theoretical results differ only in finer details.[10] Therefore our focus is to examine ac-conductivity data in a broader context rather than within the confines of a particular theory. We have approached this goal by adopting generalized parameters, and by utilizing the simplest ac conductivity theory for a semiquantitative analysis of specific ac conductivity features.

II. EXPERIMENTAL DETAILS

Experiments were conducted between 75 and 300 K in a standard, pseudo-four-probe configuration on an HP 4192A impedance analyzer operating over the 5-Hz–13-MHz frequency range. The experimental setup was interfaced with an HP 85 computer for data collection. Experimental details are available elsewhere.[16] Contributions from parasitic elements were evaluated by measuring a set of known resistive and capacitive elements in various configurations, as described in Ref. 16. All the reported data in the present report have been subjected to this correction.

Single crystals were grown as described elsewhere.[6] The samples were cut in the shape of parallelepipeds in the a-b plane, typically about 0.5 cm in length and 0.010 cm^2 in cross section. The samples were annealed for 24 h to attain the desired δ values, as prescribed in Ref. 7, and drop quenched. Samples with δ values 0.01, 0.03, 0.06, and 0.08 in the single phase region were kept in mineral oil and ex-

 © 1996 The American Physical Society

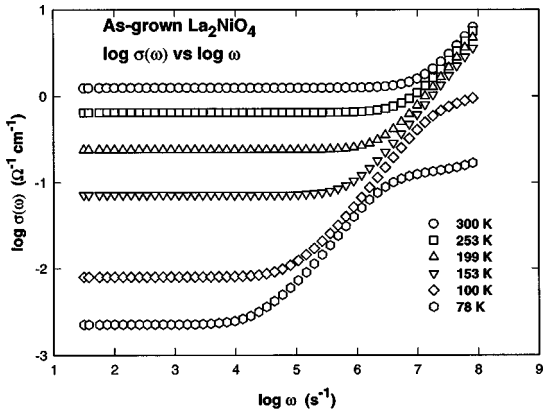

FIG. 1. $\log_{10}\sigma(\omega)$ vs $\log_{10}\omega$ plots for the as-grown sample at various values of T.

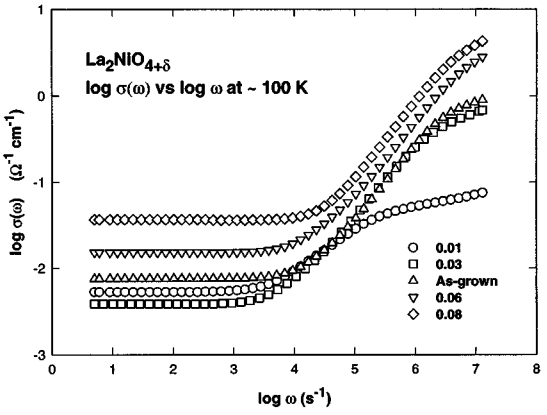

FIG. 2. $\log_{10}\sigma(\omega)$ vs $\log_{10}\omega$ plots for all samples at ~100 K.

periments conducted within a time span of 24 h. The as-grown sample, included in the present investigation, has a composition close to $\delta\approx 0.05$. Contacts to the sample ends were made with indium, electrically connected to the ac conductivity leads using silver paint. Utmost precautions were taken to ensure good Ohmic contacts: bad contacts resulted in erratic impedance behavior as temperature was lowered. Such data sets were discarded, and the experiment was repeated on a fresh sample. Data at 5-Hz matched data taken by four-probe dc measurements. All reported data were collected during the first cooling cycle.

III. RESULTS AND DISCUSSION

We first plot the ac conductivity $\sigma(\omega)$ $[=\sigma_1(\omega)+i\sigma_2(\omega)$, where subscripts 1 and 2 denote the real and imaginary components], at selected temperatures as a function of frequency ω. The representative $\log_{10}\sigma(\omega)$-$\log_{10}\omega$ plots at various values of T for the as-grown sample are displayed in Fig. 1. The key features are listed below: (i) The $\log_{10}\sigma(\omega)$-$\log_{10}\omega$ curves are flat in the low-frequency region $\sigma(\omega)\approx\sigma_{dc}[\equiv\sigma(0)\approx\sigma(5\text{ Hz})]$. The ac conductivity in the dispersive region follows an approximate power law $\sigma(\omega)\propto\omega^s$ $(0<s<1)$. (ii) $\sigma(\omega)$ finally saturates at ω_s or becomes very weakly frequency dependent. (iii) After $\sigma(\omega)$ rises from its dc value, its temperature dependence weakens as the frequency increases; this is evidenced by the crowding of the $\log_{10}\sigma(\omega)$-$\log_{10}\omega$ curves in the high-frequency region. The conductivity ratio $\sigma(10\text{ MHz})/\sigma(0)$ is strongly temperature dependent. (iv) The shape of the $\log_{10}\sigma(\omega)$-$\log_{10}\omega$ curves is similar for various temperatures.

Additional characteristic signatures of the ac conductitivy emerge from Fig. 2, which is a $\log_{10}\sigma(\omega)$-$\log_{10}\omega$ plot near 100 K for various δ: (vi) The shape of the curves is similar for all δ at fixed T. (vii) The critical frequency ω_c at which $\sigma(\omega)$ begins to rise from its dc value decreases with $\sigma(0)$. For a fixed δ value, ω_c decreases with temperature (Fig. 1). We now discuss these key ac-conductivity features in the context of our data on $La_2NiO_{4+\delta}$ in further detail.

A. ω and T dependence of ac conductivity

1. Frequency exponent s

The Austin-Mott[9] equation for ac conductivity is approximated by $\sigma(\omega)\propto\omega^s$. The frequency exponent s is defined as

$$s\equiv d\ \ln\sigma(\omega)/d\ln\ \omega, \tag{1a}$$

which yields

$$s=1-4/\ln(\nu_{ph}/\omega). \tag{1b}$$

Here ν_{ph} is a fundamental rate constant (of the order of a phonon frequency $\approx 10^{12}$–10^{13} s^{-1}). For a particular dispersive curve, s depends on ω, principally through the transition to dc conduction at low ω and to saturation at high ω. Hence we find it convenient to define an average s, s_{av}, with a corresponding average frequency ω_{av} at the midpoint of the dispersion range, which is well separated from the transition regions.

The temperature dependence of s_{av} is complex: According to Eq. (1b), s depends on how ν_{ph} changes with T. It is often overlooked that s may further change with T because the midpoint of the dispersive region moves to lower frequencies as the temperature is lowered (Fig. 1); this results in a corresponding increase in s_{av} [Eq. (1b)]. Thus in the Austin-Mott formula the details of the s_{av}-T relationship are intimately linked to the variation of ν_{ph} with T, as well as to the T dependence of the dispersion characteristics, and are difficult to predict.

In Fig. 3, s_{av} vs T values are displayed for all δ. For all samples except for $\delta=0.01$, s_{av} varies between 0.6 and 0.85, as is found for many cases of interest,[17] including $La_2CuO_{4+\delta}$.[5] Further, s_{av} increases with δ except for

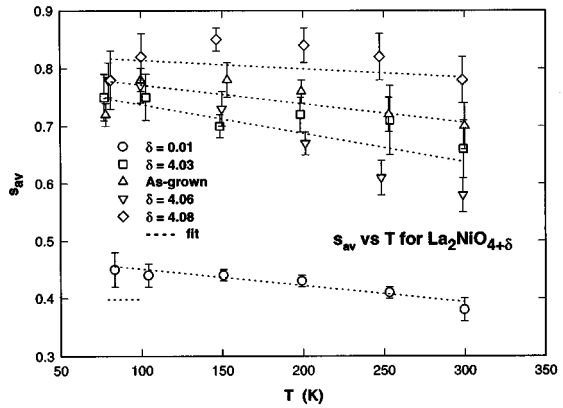

FIG. 3. s_{av} vs T variations together with least-squares fits (see text).

δ=0.06; a trend to the contrary was reported for the Cu analog.[5] However, the T dependence of s_{av} is complex: the weak T dependence of s_{av}, as computed from the movement of the dispersion region to lower frequencies, is indicated by the least-squares fit in Fig. 3 (broken line). For the δ=0.03 and 0.08, and for the as-grown sample, we could assume that ν_{ph} is independent of T and that it increases from $\sim 10^{12}$ to 10^{15} s^{-1}, respectively; a value of 10^{12} s^{-1} is found for impurity conduction in Ge.[18] For δ=0.06, the comparatively steep s_{av}-T curve cannot easily be reproduced, even with an exponential T dependence of ν_{ph}. For δ=0.01, s_{av} remains exceptionally small between 0.38 and 0.45 at all temperatures. For this sample an additional dependence of ν_{ph} on T must be invoked to simulate the s_{av}-T behavior, shown by the broken line in Fig. 3. We also note that for this sample the ratio σ(10 MHz)/σ(0) is small and the dispersion region is narrow; both ω_c and ω_s have rather low values; see Fig. 2.

2. Saturation with ω

Saturation or near saturation is observed in $\sigma(\omega)$ at about 100–200 K in the frequency range of our measurements; at a fixed frequency the lower the δ value the higher is the onset temperature of saturation. This may be seen in Fig. 2 by noting that for δ=0.01 saturation is already encountered at low frequencies, whereas for δ=0.08 it has barely set in.

This appears to be the first report of saturation in the radio frequency range in an electronic system. A similar plateau in the frequency response of $\sigma(\omega)$ in the range 10^3–10^6 Hz was observed in a Czochralski-grown single-crystal alumina sample at high T (1323–1623 K), subjected to an oxygen partial pressure of 2×10^{-2} to 1 atm;[19] under these conditions ionic conduction is presumed to dominate.

3. T dependence of ac conductivity

From the T dependence of the various terms in the Austin-Mott[9] formula, a weak, non Arrhenius T dependence of the ac conductivity $\sigma(\omega)\propto T^t$ is predicted ($0\leqslant t\leqslant 1$). The absence of an exponential T dependence of $\sigma(\omega)$, and the weak T dependence observed in our data, strongly suggest that hopping transport involves localized states with energies within k_BT of the Fermi level.[18] This is further inferred by the strongly T-dependent σ(10 MHz)/σ(0) ratio. These features are in striking contrast to hopping phenomena in band tails for which an Arrhenius-type T dependence of the ac conductivity and an associated nearly T-independent conductivity ratio is observed, as for example in AsF_5-doped polyphenylacetate.[20]

B. Scaling characteristics

We next concentrate on the scaling properties of our data. Summerfield[21] noted (from data for diverse systems such as amorphous and doped semiconductors) that the ac conductivity tends to be universal function of a reduced frequency, which contains T and $\sigma(0)$ as important parameters. The *reduced ac conductivity* $\sigma(\omega)/\sigma(0)$ scales with *reduced frequency*, $\tilde{\omega}/\tilde{\sigma}(0)$;[21] here $\tilde{\omega}\equiv\omega/R_0$ and $\tilde{\sigma}(0)\equiv\sigma(0)k_BT/\alpha R_0e^2$. R_0 is a transition rate preexponential factor, and α is the spatial wave-function decay parameter of the localized states. Other symbols have their conventional meaning.

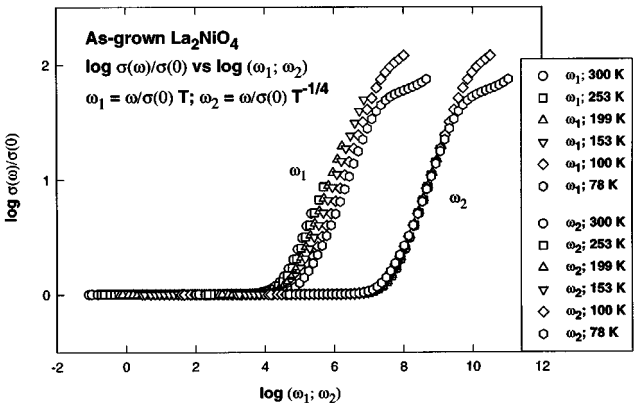

FIG. 4. $\log_{10}\sigma(\omega)/\sigma(0)$ vs $\log_{10}\omega_n$ plots illustrating scaling with T (78–300 K). $n=1$, $\omega_{red}\equiv\omega_1$; $n=-\frac{1}{4}$, $\omega_{red}\equiv\omega_2$.

We enlarge on the universality properties of our data by combining the *reduced ac conductivity* $\sigma(\omega)/\sigma(0)$ with a *generalized reduced frequency*[22]

$$\omega_{red}\equiv\omega_{/}=\omega/(\sigma(0)T^n), \tag{2}$$

where n is a fitting parameter. This generalized form will be used below to examine scaling with respect to T (at fixed composition) and to composition (at fixed T).

1. Scaling with T

We first consider scaling with respect to T at a fixed composition δ. Representative reduced data are displayed in Fig. 4 for the as-grown sample, as $\log_{10}\sigma(\omega)/\sigma(0)$ versus $\log_{10}\omega_{/}$ curves for $n=1$ and $-\frac{1}{4}$; in this figure, $\omega_n\equiv\omega_1$ for $n=1$, and $\omega_n\equiv\omega_2$ for $n=-\frac{1}{4}$. For $n=1$, the reduced curves do not overlap very well; this is also the case for all other samples. For $n=0$, the lower-T reduced curves remain shifted to the right (as for $n=1$ in Fig. 4), though to a much lesser extent. However, as is illustrated in Fig. 4, an excellent universality plot is obtained for $n=-\frac{1}{4}$ up to $\log_{10}\omega_2\sim 9.5$. The superposition deteriorates below 100 K for frequencies exceeding 1 MHz; this may be related to saturation of $\sigma(\omega)$ in this ω-T region. The same degree of universality is encountered for samples with δ=0.06 and 0.08. By contrast, for samples with δ=0.01 and 0.03, excellent scaling is obtained over the entire measured frequency and temperature range, including the saturation region. The empirical n values fall between $-\frac{1}{3}$ and $-\frac{1}{4}$ for $\sigma(\omega)/\sigma(0)\leqslant 100$. Reported literature values for n range from 1 [$\sigma(\omega)/\sigma(0)\leqslant 10^8$] for heavily doped n-type Si and V_2O_5-P_2O_5 glasses,[11] to 0.57 for Au-doped amorphous Si [$\sigma(\omega)/\sigma(0)\leqslant 100$],[22] to 0 for amorphous Ge and Si [$\sigma(\omega)/\sigma(0)\leqslant 10$].[10] The above analysis indicates that for $La_2NiO_{4+\delta}$ n is negative and obviously system dependent.

Interpretation of n. Hunt[23] noted that if experimental data obey the relation, $\omega_{red}\propto\omega/\sigma(0)T^p$, then T^{-p} is to be identified as the appropriate preexponential factor in $\sigma(0)$. Hunt illustrated such a correlation for Au-doped amorphous Si as reported by Long and Hansmann.[22] p varies from system to system, as the various reported data analyses reveal.[10,11,22] For our scaled data for the as-grown sample, $p=n=-\frac{1}{4}$, in close agreement with the theoretical preexponential factor

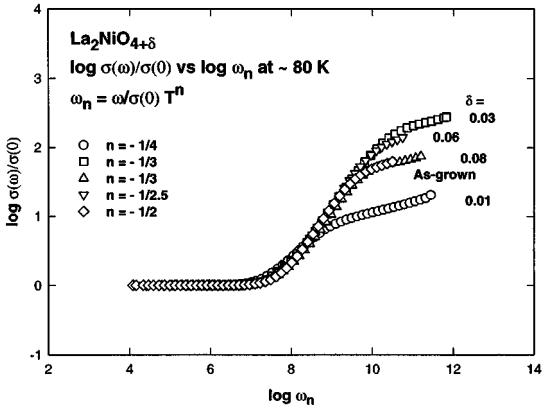

FIG. 5. $\log_{10}\sigma(\omega)/\sigma(0)$ vs $\log_{10}\omega_n$ plots demonstrating universality with changing compositions at ~80 K. $\omega_{\rm red}\equiv\omega_n$; n varies from $-\frac{1}{4}$ to $-\frac{1}{2}$.

$T^{1/4}$ for hopping transport, which we encounter in the data below our critical frequency.

2. Scaling with composition

Dyre[14] first reported that ac conductivity additionally scales with chemical composition. This was illustrated by him for a number of diverse systems; however, compositional scaling has seldom been explored. For our purposes the compositional parameter is implicit in the variation of $\sigma(0)$ in Eq. (2) with changing composition.

We examine scaling with respect to composition via adjustment of $\sigma(0)$ (that is, variation of δ) at a fixed T. The *generalized reduced frequency* [Eq. (2)] now contains $\sigma(0)$ and n as variables instead of T. n in Eq. (2) has been suitably adjusted to achieve the superposition displayed in Fig. 5. Only minor alterations are required to achieve complete scaling below saturation: $n=-\frac{1}{4}$, $-\frac{1}{3}$, $-\frac{1}{3}$, $-1/2.5$, and $-\frac{1}{2}$ for δ=0.01 and 0.03, as-grown, and 0.06 and 0.08, respectively, at about 80 K. In the saturation region, the reduced curves are very similar in appearance, but they do not overlap; this breakdown of scaling is expected, as mentioned below.

3. Summerfield scaling law

Up to this point we have emphasized scaling, using a generalized form, which leads to the superposition of data at various values of T (Fig. 4) and at several compositions (Fig. 5). We now specifically examine the degree to which individual data sets agree with the Summerfield scaling law. This procedure also yields an estimate of α.

Summerfield found that ac-conductivity data are well represented by an empirical scaling law[21]

$$\sigma(\omega)/\sigma(0)=f(A\tilde{\omega}/\tilde{\sigma}(0))\equiv f(A\omega\alpha e^2/\sigma(0)k_BT), \quad (3a)$$

$$f(x)\approx 1+x^b \quad \text{with} \quad b=0.725, \quad (3b)$$

where A is a model-dependent constant. In the high-frequency limit and over an extended temperature range, the scaling breaks down. In this approach, $s_{\rm av}$ depends only on the conductivity ratio, and is not identified with a distribution of hopping rates, as in the pair approximation.

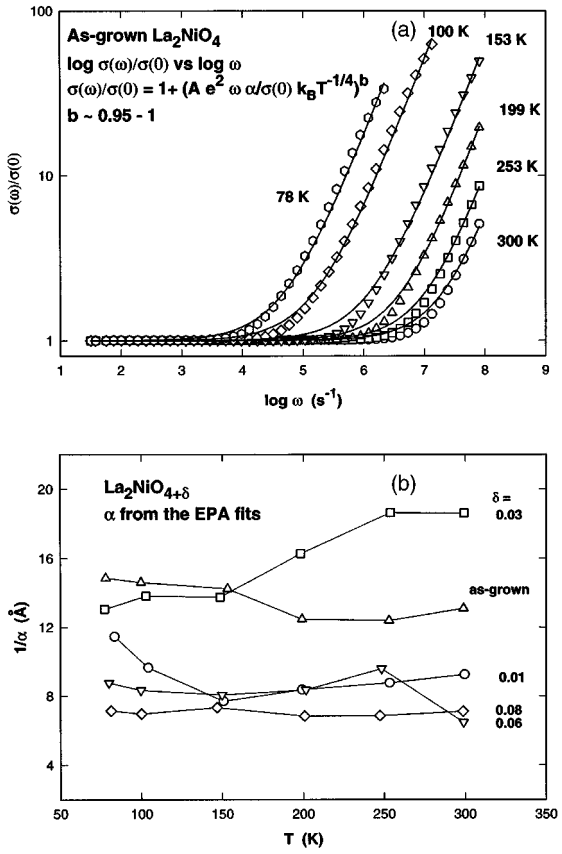

FIG. 6. (a) $\sigma(\omega)/\sigma(0)$ vs $\log_{10}\omega$ plots at various values of T (open symbols), displayed together with the EPA fits from Eqs. (3a) and (3b) (solid line). See text. (b) $1/\alpha$ vs T variation for all δ; α is determined form the EPA fits. Refer to (a) and text.

First, we discarded data in the saturation region which is not covered by the scaling law. Second, we replaced T by T^n in the denominator of Eq. (3a) for generalization, and utilized n values consistent with the ac conductivity T scaling. We adopted a nonlinear least-squares fitting procedure to obtain a best fit to the data. The resulting EPA curves and data for the as-grown sample are displayed in Fig. 6(a). There is fairly good agreement between the data and the EPA results (solid line), except in the transition region; similar fits were found for all other δ. The fitting parameter b of Eq. (3b) falls between 0.9 and 1, except for δ=0.01, where b varies from 0.64 to 0.76 [due to slight variations of the $\log_{10}\sigma(\omega)$-$\log_{10}\omega$ curves with T at the onset of dispersion]. From the EPA fits an estimate of the localization lengths $1/\alpha$ is obtained; these range from 6 to 18 Å, which are reasonable values close to those quoted by Summerfield[21] for amorphous Ge. In Fig. 6(b), we display $1/\alpha$ vs T plots for all δ; a similar weak T dependence is also encountered in other hopping systems, but is not well understood at present.

C. Loss peak at ω_c

1. Peaks in the normalized ac-conductivity functions F_r and F_i

A loss peak is an essential feature of hopping transport;[10,11] however, spatial inhomogeneity may also give

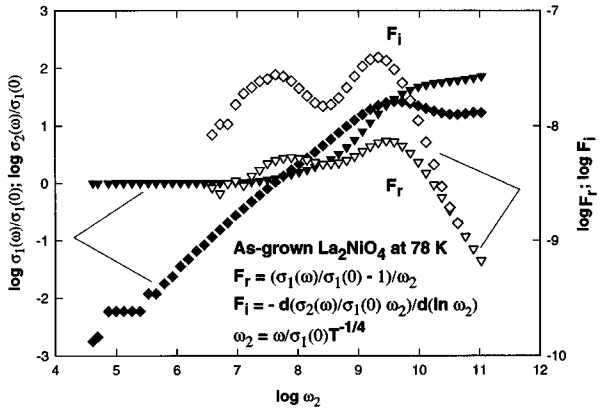

FIG. 7. $\log_{10}\sigma_1(\omega)/\sigma_1(0)$ and $\log_{10}\sigma_2(\omega)/\sigma_1(0)$ vs $\log_{10}\omega_2$ plots (solid symbols) for the as-grown sample at ~78 K are displayed. Note the two crossover points. Also included are plots of $\log_{10}F_r$ and $\log_{10}F_i$ vs $\log_{10}\omega_2$ (open symbols), which show peaks in the vicinity of the crossover points.

rise to such structures, as pointed out in Ref. 10. Such signatures are well established; they have been seen in lossy dielectrics and insulators, as well as in glasses, for many years.[10,11,24] They were first theoretically predicted for electron hopping (as opposed to Debye relaxation phenomena) by Bryksin,[25] who found a loss peak in the vicinity of ω_c. Other hopping models have since yielded similar results.[10] This feature can be clearly seen in the two normalized conductivity functions F_r and F_i, which are model independent. These functions are defined below:[10]

$$F_r=[(\sigma_1(\omega)/\sigma_1(0))-1]/\omega_n, \tag{4a}$$

$$F_i=-d(\sigma_2(\omega)/\sigma_1(0)\omega_n)/d(\omega_n). \tag{4b}$$

Plots depicting $\log_{10}F_r$ and $\log_{10}F_i$ vs $\log_{10}\omega_2$ [again, $\omega_n\equiv\omega_2$ for $n=-\frac{1}{4}$ in Eq. (2) for a generalized reduced frequency] for the as-grown sample at 78 K are displayed in Fig. 7. Also included in this figure are $\log_{10}\sigma_1(\omega)/\sigma_1(0)$ and $\log_{10}\sigma_2(\omega)/\sigma_1(0)$ vs $\log_{10}\omega_2$ curves. The salient features are the following: (i) The $\log_{10}\sigma_1(\omega)/\sigma_1(0)$ and $\log_{10}\sigma_2(\omega)/\sigma_1(0)$ versus $\log_{10}\omega_2$ curves cross over at two frequencies ω_- and ω_+ near the two peaks in the $\log_{10}F_r$ and $\log_{10}F_i$ versus $\log_{10}\omega_2$ curves. (ii) The first loss peak occurs near the frequency of the onset of dispersion (ω_c), below which $\sigma_2(\omega)/\sigma_1(0)$ is proportional to ω. (iii) The second crossover (loss peak) occurs near the onset of saturation in ac conduction. (iv) Both F_r and F_i are similar in shape; the former is smaller by a factor of 10.

Tentatively, we associate the second loss peak with the saturation of $\sigma(\omega)$ and determine the saturation frequency from the location of the second loss peak or from the corresponding crossover point. Because saturation is not normally encountered, to our knowledge this is among the first observations of a second loss peak.

The above-mentioned features in $La_2NiO_{4+\delta}$, except those due to saturation, are commonly encountered in systems involving localized carriers.[10] Since our 5-Hz resistivity data suggest variable range hopping, hopping transport, not inhomogeneity, is deemed to be the underlying cause for the

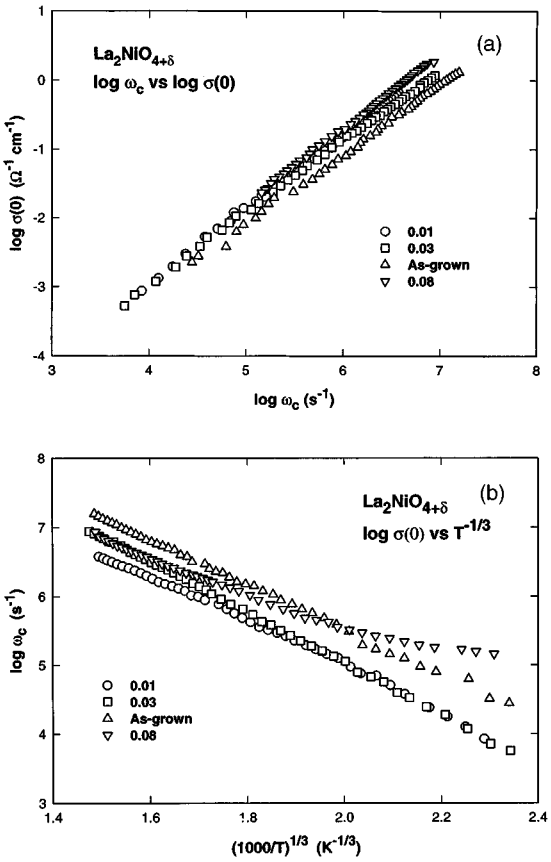

FIG. 8. (a) $\log_{10}\omega_c$ vs $\log_{10}\sigma(0)$ plots for various values of δ illustrating the $\sigma(0)\propto\omega_c$ proportionality. (b) $\log_{10}\omega_c$ vs $(1000/T)^{1/3}$ plots for several δ values.

loss peaks. Further corroboration is found in the correlation of $\sigma(0)$ and ω_c and their functional dependence on T, as discussed below.

2. Critical frequency ω_c versus $\sigma(0)$ and T

A well-known proportionality $\sigma(0)\propto\omega_c$ is observed in all other systems characterized by hopping transport.[11] The critical frequency as determined from the peak in the measured imaginary part of the impedance $\mathrm{Im}(Z)$ is close to the crossover point, and is displayed as $\log_{10}\sigma(0)$ vs $\log_{10}\omega_c$ plots in Fig. 8(a); the linearity of these curves indicates that $\sigma(0)\propto\omega_c$ for $La_2NiO_{4+\delta}$. We further find that $\log_{10}\omega_c \propto T^{-1/3}$ as displayed in Fig. 8(b) for several values of δ. A curvature in the data for $\delta=0.08$ is evident, indicating more complex behavior in this case. The value of ν_{ph} is estimated to be $\sim10^{11}$–10^{12} s^{-1}, close to that encountered in impurity-doped Ge.[18] Due to the proportionality between $\sigma(0)$ and ω_c, we may assume that $\sigma(0)\propto T^{-1/3}$. This is consistent with the aforementioned result of Ref. 8, and indicates that both the dc and ac transport processes involve the same mechanism.

IV. CONCLUSIONS

Our ac-conductivity data on $La_2NiO_{4+\delta}$ exhibit the following set of signatures: (i) The ac conductivity follows a ω^s power law ($s\sim0.38$–0.85). (ii) At higher values of ω, a saturation in frequency response is encountered. (iii) Beyond ω_c, the ac conductivity displays a weak T dependence. (iv)

The reduced ac-conductivity data at various values of T scale with the reduced frequency. (v) The reduced ac-conductivity data for various δ at a fixed T lie on a universal curve. (vi) ac conductivity may be treated by the Summerfield scaling law. (vii) Two loss peaks are observed in the normalized conductivity functions. These occur in the vicinity of ω_c and ω_s. (viii) $\sigma(0) \propto \omega_c$, with $\omega_c \propto \exp[(-T_2/T)^{1/3}]$. Below ω_c, $\sigma_2(\omega)/\sigma(0) \propto \omega$.

The above ac characteristics (except the saturation plateau) bear a close resemblance to those encountered in amorphous- and impurity-doped semiconductors. These also meet all the criteria expected from hopping transport in an electronic material.

One of the important conclusions of the present investigation is that localized charge carriers at the Fermi level must be present in $La_2NiO_{4+\delta}$ at densities ($\sim 3\times 10^{22}$ states/cm^{3}eV) sufficient to produce the very significant dispersion effects summarized above. Any itinerant electrons also present are not detected by ac techniques at frequencies up to 10 MHz. In the earlier literature, transport phenomena were generally discussed in terms of itinerant charge carriers.[6] However, several observations reported in the literature lead to the conclusion that $La_2NiO_{4+\delta}$ is a polaronic or Anderson-localized material. Among these measurements are soft-x-ray absorption and emission studies,[26] photoemission work,[27] electron-diffraction experiments,[28] infrared-absorption measurements,[29] neutron-diffraction studies,[30] magnetization measurements,[31,32] and electron-transport phenomena.[32,33] A number of theoretical presentations are also based on electron localization.[34,35] On taking all of this work into account, one is forced to the conclusion that most, if not all, charge carriers in the $La_2NiO_{4+\delta}$ system are localized, and require a thermal or optical activation energy to move from site to site.

ACKNOWLEDGMENTS

We gratefully acknowledge the technical assistance of P. Metcalf, and illuminating discussions with Professor F. A. Chudnovskii. This project was conducted with the financial assistance of a National Science Foundation Grant No. DMR 92-22986, and a Department of Energy Grant No. DE-FG02-90ER452427.

*Present address: Department of Physics, University of Oregon, Eugene, OR 97403.

†Permanent address: Department of Physics, Department of Natural Sciences, Pukyong National University of Technology, Namgu, Pusan 608-73, Korea.

[1] M. A. Kastner *et al.*, Phys. Rev. B **37**, 111 (1988).

[2] N. W. Preyer *et al.*, Phys. Rev. B **39**, 11 563 (1989).

[3] C. Y. Chen *et al.*, Phys. Rev. B **51**, 3671 (1995).

[4] Th. Strangfeld, K. Westerholt, and H. Bach, Physica C **183**, 1 (1990); X. Granados *et al.*, J. Solid State Chem. **102**, 455 (1993).

[5] C. Y. Chen *et al.*, Phys. Rev. Lett. **63**, 2307 (1989).

[6] D. J. Buttrey and J. M. Honig, in *The Chemistry of High Temperature Superconductors*, edited by C. N. R. Rao (World Scientific, Singapore, 1991), and references therein.

[7] R. R. Schartman, Ph.D. thesis, Purdue University, 1989.

[8] R. J. Rasmussen (private communication).

[9] I. G. Austin and N. F. Mott, Adv. Phys. **18**, 41 (1969).

[10] A. R. Long, in *Hopping Transport in Solids*, edited by M. Pollak and B. Shklovskii (North-Holland, Amsterdam, 1991), p. 207, and references therein.

[11] J. C. Dyre, J. Appl. Phys. **64**, 2456 (1988), and references therein.

[12] H. Böttger and V. V. Bryksin, *Hopping Conduction in Solids* (VCH Verlagsgesellschaft, Weinheim, 1985).

[13] S. Summerfield and P. N. Butcher, J. Phys. C **15**, 7003 (1982).

[14] J. C. Dyre, Phys. Lett. **108A**, 457 (1985).

[15] A. Hunt, J. Phys. Condens. Matter **4**, 6957 (1992), and references therein.

[16] R. J. Rasmussen, Ph.D. thesis, Purdue University, 1988.

[17] R. M. Hill and A. K. Jonscher, J. Non-Cryst. Solids **32**, 53 (1979).

[18] N. F. Mott and E. A. Davis, *Electronic Processes in Non-Crystalline Materials* (Clarendon, Oxford, 1971).

[19] H. M. Kizilyalli and P. R. Mason, Phys. Status Solidi A **36**, 499 (1976).

[20] A. P. Bhatt, W. A. Anderson, and P. Ehrlich, Solid State Commun. **47**, 997 (1983).

[21] S. Summerfield, Philos. Mag. B **52**, 9 (1985).

[22] A. R. Long and L. Hansmann, in *Hopping and Related Phenomena*, edited by H. Fritzsche and M. Pollak (World Scientific, Singapore, 1990), p. 77.

[23] A. Hunt, Philos. Mag. B **64**, 579 (1991).

[24] J. C. Dyre, J. Non-Cryst. Solids **135**, 219 (1991).

[25] V. V. Bryksin, Sov. Phys. Solid State **22**, 1421 (1980).

[26] S. M. Butorin *et al.*, Physica C **235–240**, 1047 (1994).

[27] H. Eisaki *et al.*, Phys. Rev. B **45**, 12 513 (1992).

[28] C. H. Chen, S.-W. Cheong, and A. S. Cooper, Phys. Rev. Lett. **71**, 2461 (1993).

[29] X.-X. Bi, P. C. Eklund, and J. M. Honig, Phys. Rev. B **42**, 4756 (1990).

[30] J. M. Tranquada *et al.*, Phys. Rev. Lett. **73**, 1003 (1994).

[31] K. Yamada *et al.*, Physica C **221**, 355 (1994).

[32] S.-W. Cheong, Phys. Rev. B **49**, 7088 (1994).

[33] S. Nishiyama, D. Sakaguchi, and T. Hattori, Solid State Commun. **94**, 279 (1995).

[34] J. Zaanen and P. B. Littlewood, Phys. Rev. B **50**, 7222 (1994).

[35] H. Roder, H. Fehske, and R. N. Silver, Europhys. Lett. **28**, 257 (1994).